

Symmetric localization of $\nu_{\text{tot}} = 4/3$ fractional topological insulator edges

Yang-Zhi Chou ^{1,*} and Sankar Das Sarma¹

¹*Condensed Matter Theory Center and Joint Quantum Institute,
Department of Physics, University of Maryland, College Park, Maryland 20742, USA*
(Dated: March 12, 2026)

Motivated by the recent twisted MoTe₂ experiment [arXiv:2601.18508], we develop a disordered interacting edge theory of a fractional topological insulator at $\nu_{\text{tot}} = 4/3$, consisting of two time-reversal-conjugated $\nu = 2/3$ fractional quantum Hall states. For an S_z -conserving edge, we uncover three distinct phases with two possible conductance values per edge in the long-edge limit: $\frac{2}{3} \frac{e^2}{h}$ and $\frac{4}{3} \frac{e^2}{h}$. In the presence of S_z -changing perturbations (e.g., Rashba spin-orbit coupling), an interaction-induced insulating edge state can emerge without breaking time-reversal or charge-conservation symmetry, corresponding to the absence of a topologically protected edge state. We further provide an exact mapping to a noninteracting fermionic theory exhibiting Anderson localization. Our results showcase an explicit, experimentally relevant example that the edge-state two-terminal transport is insufficient to identify the $\nu_{\text{tot}} = 4/3$ fractional topological insulators.

Introduction. — Fractional topological insulators (FTIs) are strongly correlated gapped states that support fractionalized excitations while preserving time-reversal symmetry and charge conservation [1–3]. (See reviews [4–6] and the references therein.) In two dimensions, the edge state of an FTI is described by fractionalized movers that form Kramers pairs, which can lead to a nontrivial two-terminal edge-state conductance. In addition, the edge states of two-dimensional (2D) FTI can be useful for engineering the parafermion zero modes [7, 8], a potential building block for topological quantum computations [9]. Despite extensive theoretical studies of FTIs, decisive evidence in the materials has remained elusive after two decades of exploration.

During the past few years, the moiré transition metal dichalcogenides have become a promising platform for exploring the interplay between topology and correlation [10–16], owing to the tunable spin-valley-locked moiré valence bands with nonzero Chern numbers. For example, fractional quantum anomalous Hall effect has been observed in the twisted MoTe₂ with $\theta \approx 3.7^\circ$ [17–21], and a possible half-integer fractional quantum spin Hall effect was reported at hole doping $\nu_{\text{tot}} = 3$ of a $\theta = 2.1^\circ$ twisted MoTe₂ [22] (ν_{tot} is the number of carrier per moiré unit cell). The fractional quantum spin Hall experiment has motivated a number of theoretical studies [23–34], but subsequent experiments found time-reversal breaking [35–38], ruling out the time-reversal FTI possibility. A very recent pump-probe circular dichroism experiment suggests a time-reversal symmetric (TRS) correlated state at $\nu_{\text{tot}} = 4/3$ in twisted MoTe₂ [39], consistent with a 2D FTI made of a pair of time-reversal conjugated $\nu = 2/3$ fractional quantum Hall (FQH) states – a possibility predicted theoretically in Ref. [31]. Nevertheless, the transport signature, which is a standard and important tool for identifying two-dimensional electronic topological phases, has not yet been experimentally verified.

In this work, we study the edge state of a 2D FTI at $\nu_{\text{tot}} = 4/3$, made of a time-reversal pair of $\nu = 2/3$ FQH

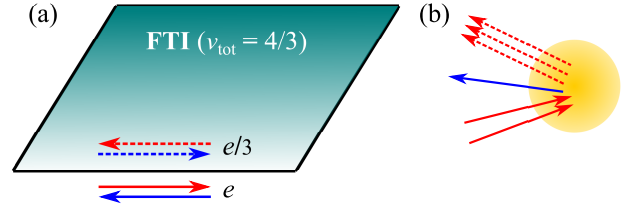


FIG. 1. (a) The edge configuration of $\nu_{\text{tot}} = 4/3$ FTI. The solid arrows indicate the charge- e movers, and the dashed arrows indicate the charge- $e/3$ movers. The blue arrows can be viewed as the edge state of a spin-up $\nu = 2/3$ FQH insulator; the red arrows can be viewed as the edge state of a spin-down $\nu = -2/3$ FQH insulator. (b) Illustration of the backscattering process $L_{\uparrow}^{\dagger} R_{\uparrow} L_{\downarrow}^{\dagger} R_{\downarrow}$ in $\mathcal{S}_{I,\text{loc}}$ [Eq. (7)]. Note that L_{\uparrow}^{\dagger} is made of three $e/3$ quasiparticles (the three red dashed lines). The interaction in $\mathcal{S}_{I,\text{loc}}$ leads to a symmetric localized state in the strong coupling limit.

states, as sketched in Fig. 1(a). We analyze the possible phases driven by TRS perturbations and provide the corresponding two-terminal edge-state conductance in the long edge length limit. See Table I for a brief summary of the two-terminal conductance. Remarkably, we point out that an interaction-induced symmetric localized edge state can emerge from a generic edge state (i.e., without enforcing S_z conservation) and provide an exact mapping to a noninteracting fermionic theory manifesting Anderson localization. The responsible interaction backscattering is illustrated in Fig. 1(b). Our results suggest that the two-terminal edge-state conductance is insufficient to provide a decisive signature of $\nu_{\text{tot}} = 4/3$ FTI, implying the need for novel characterizations for the search for FTIs.

Edge theory as chiral bosons. — We consider a 2D product topological order at $\nu_{\text{tot}} = 4/3$ consisting of two $\nu = 2/3$ FQH states that form a time-reversal pair. Without loss of generality, we assume the spin-up electrons form a FQH state with a Hall conductivity $\sigma_H = (2/3)e^2/h$ and the spin-down electrons form a

Perturbation	$ \Delta S_z $	\mathcal{N}	G (e^2/h)
None	N/A	4	4/3
$\mathcal{S}_{I,M}$ [Eq. (4)]	0	4	2/3
$\mathcal{S}_{I,+}$ [Eq. (5)]	0	2	2/3
$\mathcal{S}_{I,J}$ [Eq. (6)]	0	2	4/3
$\mathcal{S}_{I,\text{loc}}$ [Eq. (7)]	1	0	0

TABLE I. Summary of different phases of FTI edge states. We list the properties of each phase driven by the associated perturbation in the strong-coupling limit. $|\Delta S_z|$ indicates the change of S_z during the scattering, \mathcal{N} denotes the number of low-energy modes, and G_∞ indicates the two-terminal conductance per edge in the infinite edge length limit.

FQH state with a Hall conductivity $\sigma_H = -(2/3)e^2/h$, with the edge state structure shown in Fig. 1(a). Based on exact diagonalization, this state is the ground state of the twisted MoTe₂ at hole doping $\nu_{\text{tot}} = 4/3$ [31, 39]. In addition, this topological order is minimal with the smallest quantum dimension [24, 40]. Using the chiral boson description [41–43], the imaginary-time action for the quadratic boson theory is given by

$$\mathcal{S}_0 = \frac{1}{4\pi} \int_{\tau,x} (\partial_x \Phi^T) \left[\hat{\mathcal{K}} (i\partial_\tau \Phi) + \hat{\mathcal{V}} (\partial_x \Phi) \right], \quad (1)$$

where $\int_{\tau,x}$ is a short-hand notation for $\int d\tau dx$, Φ is a four-component column vector made of real-valued chiral boson fields, $\hat{\mathcal{K}}$ is a 4×4 K matrix encoding the commutation relations of the bosonic fields, and $\hat{\mathcal{V}}$ is a 4×4 velocity matrix describing the velocities and non-universal forward scatterings among the chiral bosons. The chiral bosons obey the following commutation relation

$$[\partial_x \Phi_a(x), \Phi_b(x')] = 2\pi i \left(\hat{\mathcal{K}}^{-1} \right)_{ab} \delta(x - x'). \quad (2)$$

For the FTI edge state considered in this work, the K matrix can be described by [43, 44]

$$\hat{\mathcal{K}} = \begin{bmatrix} \hat{K} & 0 \\ 0 & -\hat{K} \end{bmatrix}, \quad \hat{K} = \begin{bmatrix} 1 & 0 \\ 0 & -3 \end{bmatrix}. \quad (3)$$

In the above expressions, the $\hat{\mathcal{K}}$ manifestly obeys time-reversal symmetry, and \hat{K} is the K matrix for the $\nu = 2/3$ FQH state, describing a charge- e mover and a counter-propagating charge $e/3$ mover [44]. The corresponding integer-valued charge and the spin vectors given by $Q^T = [1, 1, 1, 1]$ and $S^T = [1, 1, -1, -1]$, respectively. The charge Hall conductivity is given by $\sigma_H = \nu_e \frac{e^2}{h}$, where $\nu_e = Q^T \hat{\mathcal{K}}^{-1} Q = 0$; the spin Hall conductivity is given by $\sigma_{sH} = \nu_s \frac{e}{2\pi}$, where $\nu_s = \frac{1}{2} Q^T \hat{\mathcal{K}}^{-1} S = 2/3$ [43].

In our theory, the four-component vector is $\Phi^T = [\varphi_\uparrow^R, \varphi_\uparrow^L, \varphi_\downarrow^L, \varphi_\downarrow^R]$, where φ_s^η is the chiral boson field with η chirality (R/L) and spin s . Notably, φ_\uparrow^R and φ_\downarrow^L can

be viewed as the $\nu = \pm 1$ integer quantum Hall edge states, while φ_\uparrow^L and φ_\downarrow^R are equivalent to the Laughlin quasiparticles of $\nu = \mp 1/3$. The electron field operator can be constructed by these chiral bosons, specifically, $R_\uparrow \sim e^{i\varphi_\uparrow^R}$, $L_\uparrow \sim e^{-i3\varphi_\uparrow^L}$, $R_\downarrow \sim e^{i3\varphi_\downarrow^R}$, and $L_\downarrow \sim e^{-i\varphi_\downarrow^L}$. Note that the minus signs in the exponents of the left-moving fermions are consistent with the total density operator given by $\rho_{\text{tot}} = \frac{1}{2\pi} Q^T \partial_x \Phi$. The factor of 3 for L_\uparrow and R_\downarrow indicates that annihilating a physical electron is equivalent to the destruction of three Laughlin quasiparticles. The time-reversal operation on chiral bosons are defined by [43] $(\varphi_\uparrow^R, \varphi_\uparrow^L) \rightarrow (\varphi_\downarrow^L, \varphi_\downarrow^R)$, $(\varphi_\downarrow^R, \varphi_\downarrow^L) \rightarrow (\varphi_\uparrow^L + \pi/3, \varphi_\uparrow^R + \pi)$, and $i \rightarrow -i$. One can show that the operations on fermions are given by $(R_\uparrow, L_\uparrow) \rightarrow (L_\downarrow, R_\downarrow)$, $(R_\downarrow, L_\downarrow) \rightarrow (-L_\uparrow, -R_\uparrow)$, and $i \rightarrow -i$.

The quadratic boson theory is given by \mathcal{S}_0 [Eq. (1)], describing a time-reversal pair of charge- e movers (φ_\uparrow^R and φ_\downarrow^L) and a time-reversal pair of charge- $e/3$ movers (φ_\uparrow^L and φ_\downarrow^R). Tuning the matrix elements in $\hat{\mathcal{V}}$ of Eq. (1) does not induce a phase transition of the quadratic boson theory but modifies the scaling dimension of operators. In the absence of any backscattering perturbations, the two pairs of chiral bosons are not in equilibrium [44]. As a result, the two-terminal conductance predicts $G = \frac{4}{3} \frac{e^2}{h}$ per edge state, independent of the velocity matrix $\hat{\mathcal{V}}$ [45, 46]. Next, we study the phases driven by TRS backscattering perturbations and present the corresponding two-terminal conductance in the long-edge limit.

S_z -conserving symmetry-allowed perturbations. — We investigate the symmetry-allowed backscattering perturbations (i.e., with time-reversal symmetry and charge conservation) with S_z conservation. Note that S_z conservation is *not* an exact symmetry but an approximation. We focus only on the perturbations related to one-electron and two-electron scattering processes and ignore the higher-order terms (which are likely irrelevant or sub-leading). The main results are summarized in Table I. We discuss each perturbation in detail below.

First of all, we consider spin-conserving one-electron disorder backscattering described by

$$\begin{aligned} \mathcal{S}_{I,M} &= \int_{\tau,x} \left[\eta_M(x) L_\uparrow^\dagger R_\uparrow + \eta_M^*(x) R_\downarrow^\dagger L_\downarrow + \text{H.c.} \right] \quad (4a) \\ &= \int_{\tau,x} \left[\eta_M(x) e^{i(3\varphi_\uparrow^L + \varphi_\uparrow^R)} + \eta_M^*(x) e^{-i(3\varphi_\downarrow^R + \varphi_\downarrow^L)} + \text{H.c.} \right], \quad (4b) \end{aligned}$$

where $\eta_M(x)$ is a complex-valued quenched disorder potential. For a zero-mean white-noise $\eta_M(x)$, $\mathcal{S}_{I,M}$ becomes a relevant perturbation when the scaling dimensions of $e^{i(3\varphi_\uparrow^L + \varphi_\uparrow^R)}$ and $e^{-i(3\varphi_\downarrow^R + \varphi_\downarrow^L)}$ are less than $3/2$ [47, 48]. The disorder scattering process here is analogous to that in $\nu = 2/3$ FQH edge states [44, 49, 50], which is crucial for edge equilibration [44–46, 49, 50]. When the chiral bosons are equilibrated due to the disorder scatterings (either through elastic momentum relaxation

[44, 46] or inelastic scatterings [45]), the two-terminal conductance gives $G = \frac{2}{3} \frac{e^2}{h}$ per edge state in the long edge limit. Notably, these scatterings cannot remove any low-energy modes in the strong-coupling limit, as they do not satisfy the Haldane's instability criteria [51]. See an extended discussion in Appendix A. Thus, the phase driven by strong $\mathcal{S}_{I,M}$ is adiabatic to the ballistic phase dictated by the quadratic boson theory, although the conductance quanta are different in the long-edge limit.

Besides the one-electron disorder scattering, we identify an S_z -conserving two-electron backscattering interaction, described by

$$\mathcal{S}_{I,+} = \int_{\tau,x} \left[\eta_+(x) : L_{\uparrow}^{\dagger} L_{\downarrow}^{\dagger} R_{\downarrow} R_{\uparrow} : + \text{H.c.} \right] \quad (5a)$$

$$\sim \int_{\tau,x} \left[\eta_+(x) e^{i(\varphi_{\uparrow}^R + 3\varphi_{\uparrow}^L + \varphi_{\downarrow}^L + 3\varphi_{\downarrow}^R)} + \text{H.c.} \right] \quad (5b)$$

where $\eta_+(x)$ is a complex-valued quenched disorder potential and $: A :$ denotes the normal ordering of operator A . This interaction is analogous to the charge umklapp interaction in the spinful quantum wires [48, 52] and mathematically equivalent to the \mathcal{O}_+ term in Ref. [28]. For a zero-mean white-noise $\eta_+(x)$, $\mathcal{S}_{I,+}$ becomes relevant when the scaling dimension of $e^{i(\varphi_{\uparrow}^R + 3\varphi_{\uparrow}^L + \varphi_{\downarrow}^L + 3\varphi_{\downarrow}^R)}$ is less than $3/2$ [47, 48]. The interaction here removes low-energy modes in the strong-coupling limit and induces a negative-drag correlation among the charge- e and charge- $e/3$ channels. The negative-drag correlation can be inferred from the strong-coupling constraint, $\partial_{\tau}(\varphi_{\uparrow}^R + 3\varphi_{\uparrow}^L + \varphi_{\downarrow}^L + 3\varphi_{\downarrow}^R) = 0$, which is equivalent to $j_e + 3j_{e/3} = 0$ with j_e ($j_{e/3}$) being the current in the charge- e (charge- $e/3$) channel. Using the Ohm's law and e^2/h for conductance of the charge- e channel, one can straightforwardly show $G = \frac{2}{3} \frac{e^2}{h}$ per edge. Alternatively, a conductance formalism for fractionalized edge states (which is a generalization of Ref. [53]) also yields the same result. The derived conductance here strictly holds in long-edge limit.

Finally, a Josephson coupling between the charge- e and the charge- $e/3$ channels [28] is also allowed by symmetry and is given by

$$\mathcal{S}_{I,J} = J \int_{\tau,x} \left[: R_{\downarrow}^{\dagger} L_{\uparrow}^{\dagger} L_{\downarrow} R_{\uparrow} + \text{H.c.} : \right] \quad (6a)$$

$$\sim J \int_{\tau,x} \left[e^{i(\varphi_{\uparrow}^R + 3\varphi_{\uparrow}^L - \varphi_{\downarrow}^L - 3\varphi_{\downarrow}^R)} + \text{H.c.} \right], \quad (6b)$$

where J is the coupling constant for the Josephson coupling. Different from the previous two perturbations, this scattering process satisfies momentum conservation automatically, so the spatially uniform part of the interaction dominates. As a result, $\mathcal{S}_{I,J}$ becomes relevant when the scaling dimension of $e^{i(\varphi_{\uparrow}^R + 3\varphi_{\uparrow}^L - \varphi_{\downarrow}^L - 3\varphi_{\downarrow}^R)}$ is less than 2 (instead of $3/2$ for the disordered cases) [48, 52]. Notably, the interaction here is mathematically equivalent

to the \mathcal{O}_J term in Ref. [28] and the interaction for the "neutral-mode superconductivity" among two counter-propagating $\nu = 2/3$ FQH edges [54]. The Josephson coupling $\mathcal{S}_{I,J}$ gaps out a pair of low-energy modes in the strong-coupling limit and then creates a positive-drag correlation among the charge- e and charge- $e/3$ conducting channels, which can be shown explicitly. Assuming $J < 0$, the strong-coupling constraint is given by $\varphi_{\uparrow}^R + 3\varphi_{\uparrow}^L - \varphi_{\downarrow}^L - 3\varphi_{\downarrow}^R = 2\pi \times \text{integer}$, which can be recast into the current condition $j_e - 3j_{e/3} = 0$, corresponding to a two-terminal conductance $G = \frac{4}{3} \frac{e^2}{h}$ per edge state in the long-edge limit [28].

Finally, we note the three TRS perturbations are not compatible in the strong-coupling limit [28, 43, 55, 56], so at most one perturbation manifests in the low-energy limit. (See Appendix A for a discussion.) Therefore, the S_z -conserving edge state here allows for three distinct phases with two-terminal conductance values, $\frac{2}{3} \frac{e^2}{h}$ and $\frac{4}{3} \frac{e^2}{h}$ per edge, in the long edge limit. However, S_z conservation is an approximate symmetry, and a generic edge state can allow for scatterings that change S_z with an unusual possibility of symmetric localization, as we discuss next.

Symmetric localization in generic edge states. — Now, we discuss an interesting possibility due to the presence of S_z -changing scattering processes on the edge state. First, we focus on the $|\Delta S_z| = 1$ TRS one-electron and two-electron backscattering perturbations, as they likely have larger coupling constants than other perturbations. The prominent one-electron $|\Delta S_z| = 1$ backscattering is the random Rashba spin-orbit coupling [57], which does not induce instability directly. Among the leading $|\Delta S_z| = 1$ perturbations, we identify an important two-electron interaction given by

$$\mathcal{S}_{I,\text{loc}} = \int_{\tau,x} \left[\xi(x) : L_{\uparrow}^{\dagger} R_{\uparrow} L_{\downarrow}^{\dagger} R_{\uparrow} : - \xi^*(x) : R_{\downarrow}^{\dagger} L_{\downarrow} R_{\uparrow}^{\dagger} L_{\downarrow} : + \text{H.c.} \right] \quad (7a)$$

$$\sim \int_{\tau,x} \left[\begin{array}{c} \xi(x) e^{i(2\varphi_{\uparrow}^R + 3\varphi_{\uparrow}^L + \varphi_{\downarrow}^L)} \\ - \xi^*(x) e^{-i(\varphi_{\uparrow}^R + 2\varphi_{\downarrow}^L + 3\varphi_{\downarrow}^R)} + \text{H.c.} \end{array} \right], \quad (7b)$$

where $\xi(x)$ is a complex-valued quenched disorder potential. For a zero-mean white-noise $\xi(x)$, $\mathcal{S}_{I,\text{loc}}$ becomes relevant when the scaling dimensions of $e^{i(2\varphi_{\uparrow}^R + 3\varphi_{\uparrow}^L + \varphi_{\downarrow}^L)}$ and $e^{-i(\varphi_{\uparrow}^R + 2\varphi_{\downarrow}^L + 3\varphi_{\downarrow}^R)}$ are less than $3/2$ [47, 48]. In the strong-coupling limit, $e^{i(2\varphi_{\uparrow}^R + 3\varphi_{\uparrow}^L + \varphi_{\downarrow}^L)}$ and $e^{-i(\varphi_{\uparrow}^R + 2\varphi_{\downarrow}^L + 3\varphi_{\downarrow}^R)}$ operators can simultaneously remove all the chiral bosons from the low-energy theory, resulting in an insulating state in the long edge limit. (See a discussion in Appendix A.) Remarkably, such an insulating state preserves time-reversal symmetry and charge conservation, i.e., the absence of topological protection on the boundary of an FTI. In the following, we study this insulating state by providing an exact mapping to Anderson localization of fermionic excitations.

To simplify the problem, we consider a particular choice of the velocity matrix given by

$$\hat{v} = \begin{bmatrix} v_1 & 0 & v'_1 & 0 \\ 0 & 3v_2 & 0 & 3v'_2 \\ v'_1 & 0 & v_1 & 0 \\ 0 & 3v'_2 & 0 & 3v_2 \end{bmatrix}, \quad (8)$$

where $v_1 > 0$ and $v_2 > 0$ encodes the velocity of the chiral bosons, v'_1 and v'_2 described the forward scatterings among different movers. $v'_1, v'_2 > 0$ denotes the repulsive interaction, and the stability of the bosonic theory requires that $|v'_1| < v_1$ and $|v'_2| < v_2$. The above choice ignores the coupling between the charge- e and the charge- $e/3$ channels, making them manifestly decoupled. Then, we express the chiral boson fields by the phase-like and the density-like bosonic field via $\varphi_{\uparrow}^R = \phi_1 + \theta_1$, $\varphi_{\downarrow}^L = -\phi_1 + \theta_1$, $\varphi_{\downarrow}^R = (\phi_2 + \theta_2)/3$, and $\varphi_{\uparrow}^L = (-\phi_2 + \theta_2)/3$. Using these new bosonic variables, one can straightforwardly show that the Hamiltonian (corresponding to $\mathcal{S}_0 + \mathcal{S}_{I,\text{loc}}$) is expressed by $\hat{H}_1 + \hat{H}_2 + \hat{H}_{12}$, where

$$\hat{H}_1 = \frac{u_1}{2\pi} \int dx \left[K_1 (\partial_x \phi_1)^2 + \frac{1}{K_1} (\partial_x \theta_1)^2 \right] \quad (9a)$$

$$\hat{H}_2 = \frac{\bar{u}_2}{2\pi} \int dx \left[K_2 (\partial_x \phi_2)^2 + \frac{1}{K_2} (\partial_x \theta_2)^2 \right], \quad (9b)$$

$$\hat{H}_{12} = \frac{1}{(2\pi\alpha)^2} \int dx \begin{bmatrix} \xi(x) e^{i(\phi_1 + 3\theta_1 - \phi_2 + \theta_2)} \\ -\xi^*(x) e^{i(\phi_1 - 3\theta_1 - \phi_2 - \theta_2)} + \text{H.c.} \end{bmatrix}. \quad (9c)$$

In \hat{H}_1 and \hat{H}_2 , we have introduced the velocities $u_1 = \sqrt{(v_1 - v'_1)(v_1 + v'_1)}$, $\bar{u}_2 = \sqrt{(v_2 - v'_2)(v_2 + v'_2)}/3$ and the Luttinger parameters $K_1 = \sqrt{(v_1 - v'_1)/(v_1 + v'_1)}$, $K_2 = \sqrt{(v_2 - v'_2)/(v_2 + v'_2)}$. Note that $K_1 = 1$ ($K_2 = 1$) corresponds to $v'_1 = 0$ ($v'_2 = 0$). In Eq. (9c), we have restored the factor $1/(2\pi\alpha)^2$ (with α being the ultraviolet length scale) based on the fermion-boson identity in the standard Abelian bosonization [48, 52].

In a special limit, the bosonic Hamiltonian $\hat{H}_1 + \hat{H}_2 + \hat{H}_{12}$ allows for a noninteracting fermionic description. To show this, we introduce the following fermionic fields,

$$\mathcal{R}_1 = e^{i(\phi_1 + \bar{\theta}_1)}/\sqrt{2\pi\alpha}, \quad \mathcal{L}_1 = e^{i(\phi_1 - \bar{\theta}_1)}/\sqrt{2\pi\alpha}, \quad (10)$$

$$\mathcal{R}_2 = e^{i(\phi_2 + \theta_2)}/\sqrt{2\pi\alpha}, \quad \mathcal{L}_2 = e^{i(\phi_2 - \theta_2)}/\sqrt{2\pi\alpha}, \quad (11)$$

where $\bar{\theta}_1 = 3\theta_1$, and α is an ultraviolet length scale. The Klein factors have been ignored as they are not essential to our analysis. Under the time-reversal operation, $\mathcal{R}_n \rightarrow -\mathcal{L}_n$ and $\mathcal{L}_n \rightarrow \mathcal{R}_n$, for $n = 1, 2$, similar to the helical edge state of 2D TRS topological insulators [56, 58–61]. In terms of the physical fermions, \mathcal{R}_1 and \mathcal{L}_1 are related to $R_{\uparrow}L_{\downarrow}^{\dagger}R_{\uparrow}$ and $L_{\downarrow}R_{\uparrow}^{\dagger}L_{\downarrow}$, respectively, and the expressions are reminiscent of the $\nu = 1/3$ FQH fermionic operators in the coupled-wire construction [62, 63]. The situation here is very different from

the Luther-Emergy refermionization [48, 52], where the Luther-Emergy fermions often do not have simple expressions in the physical fermionic basis.

Now, we discuss the fermionic representation of the Hamiltonian $\hat{H}_1 + \hat{H}_2 + \hat{H}_{12}$. Setting $K_1 = 1/3$, the \hat{H}_1 term [Eq. (9a)] becomes [48, 52, 64]

$$\hat{H}_1 = \frac{u_1/3}{2\pi} \int dx \left[(\partial_x \phi_1)^2 + (\partial_x \bar{\theta}_1)^2 \right] \quad (12)$$

$$\rightarrow \bar{u}_1 \int dx \left[\mathcal{R}_1^{\dagger} (-i\partial_x \mathcal{R}_1) - \mathcal{L}_1^{\dagger} (-i\partial_x \mathcal{L}_1) \right], \quad (13)$$

where $\bar{u}_1 = u_1/3$. Similarly, \hat{H}_2 [Eq. (9b)] with $K_2 = 1$ becomes

$$\hat{H}_2 \rightarrow \bar{u}_2 \int dx \left[\mathcal{R}_2^{\dagger} (-i\partial_x \mathcal{R}_2) - \mathcal{L}_2^{\dagger} (-i\partial_x \mathcal{L}_2) \right]. \quad (14)$$

\hat{H}_1 and \hat{H}_2 describes 1D fermions with linear dispersion. Tuning away from $(K_1, K_2) = (1/3, 1)$, forward-scattering interactions (e.g., Luttinger-liquid interactions) arise, making the theory not exactly solvable. Finally, the \hat{H}_{12} can be expressed by

$$\hat{H}_{12} \rightarrow \int dx \left[\bar{\xi}(x) \mathcal{L}_2^{\dagger} \mathcal{R}_1 - \bar{\xi}^*(x) \mathcal{R}_2^{\dagger} \mathcal{L}_1 + \text{H.c.} \right], \quad (15)$$

where $\bar{\xi}(x) = \xi(x)/(2\pi\alpha)$. Notably, \hat{H}_{12} represents a single-particle disorder backscattering in the fermionic basis here. Thus, $\hat{H}_1 + \hat{H}_2 + \hat{H}_{12}$ is equivalent to the two copies of TRS topological insulator edge states with TRS backscattering disorder, and Anderson localization without symmetry breaking is anticipated [60, 61].

The above mapping relies on the specific form of the velocity matrix \hat{v} given by Eq. (8) with $v'_1 = 4v_1/5$ and $v'_2 = 0$ (i.e., $K_1 = 1/3$ and $K_2 = 1$). For a general velocity matrix, the \hat{H}_1 and \hat{H}_2 gain forward-scattering interactions, which may affect the scaling dimensions of the backscattering operators. As long as the scaling dimensions of $e^{i(\phi_1 + 3\theta_1 - \phi_2 + \theta_2)}$ and $e^{i(\phi_1 - 3\theta_1 - \phi_2 - \theta_2)}$ are less than $3/2$, similar localized states are expected in the long edge limit. Thus, the symmetric localization exists for a range of parameters in the edge theory.

The absence of topological protected edge state has been pointed out by Levin and Stern [2, 4, 65] for the FTI with an even ν_s/e^* (2 in our case), where ν_s is the dimensionless spin Hall conductivity [see discussion below Eq. (3)] and e^* is the minimal charge (in the unit of e). However, explicit constructions are rare, and the backscattering perturbations may be in higher-order processes, without a transparent physical consequence for the realistic materials. Our results provide an explicit construction and a mapping to Anderson localization, showing how the symmetric insulating edge state arises in a minimal model that is relevant to the recent twisted MoTe₂ experiment [39].

Discussion. — In this work, we investigate the edge-state two-terminal conductance of a $\nu_{\text{tot}} = 4/3$ FTI, relevant to the recent twisted MoTe₂ experiment [39].

For edge states with strict S_z conservation, we find that the edge theory remains conducting for the leading S_z -conserving TRS perturbations. However, the two-terminal conductance is nonuniversal and depends on the details. For example, the one-electron disorder backscattering $\mathcal{S}_{I,M}$ [Eq. (4)] can reduce the ballistic conductance $\frac{4}{3}\frac{e^2}{h}$ to $\frac{2}{3}\frac{e^2}{h}$ per edge when equilibrium between the charge- e and charge- $e/3$ channels is achieved [44–46]. Furthermore, the interactions $\mathcal{S}_{I,+}$ and $\mathcal{S}_{I,J}$ can induce nontrivial correlation by removing a subset of the low-energy and further result in conductance quanta $\frac{2}{3}\frac{e^2}{h}$ and $\frac{4}{3}\frac{e^2}{h}$ per edge, respectively. In the long edge limit, we expect the two-terminal edge-state conductance converges to either $\frac{2}{3}\frac{e^2}{h}$ (dominant $\mathcal{S}_{I,M}$ or $\mathcal{S}_{I,+}$) or $\frac{4}{3}\frac{e^2}{h}$ (dominant $\mathcal{S}_{I,J}$) per edge, demonstrating the topological protection in the S_z -conserving edge states.

Meanwhile, S_z conservation is not exact, and the edge states have lower symmetry (e.g., absence of inversion symmetry). As a result, terms like Rashba spin-orbit coupling and “Rashba-dressed” interactions can become significant on the edge states despite the fact that S_z conservation approximately holds in the bulk. For generic edge states without S_z conservation, the $\mathcal{S}_{I,\text{loc}}$ can result in an insulating state without breaking time-reversal symmetry or charge conservation. As we discussed previously, such a TRS insulating state can be viewed as the regular Anderson localization of (dressed) edge electrons through an exact mapping to a noninteracting model. The conductance is given by $G \sim e^{-L/\xi_c}$ for $L \gg \xi_c$, where ξ_c is the localization length. Thus, the generic edge state may not be sharply distinguished from the trivial Anderson localized edge state through the standard transport measurement. Other notable S_z -changing perturbations are $|\Delta S_z| \geq 2$ processes (e.g., $L_\downarrow^\dagger R_\uparrow R_\downarrow^\dagger L_\uparrow$) and inelastic interactions [66–71]. However, the $|\Delta S_z| \geq 2$ perturbations are likely parametrically small as the approximate S_z conservation disfavors larger $|\Delta S_z|$ scatterings, and these inelastic interactions [66–71] cannot induce instability to the quadratic edge theory. Thus, we conclude that the symmetric localization due to $\mathcal{S}_{I,\text{loc}}$ is the dominant correction to the S_z -conserving edge. See Table I for a summary of the conductance in various situations.

We conclude by discussing several interesting future directions. The current work emphasizes the possible phases but ignores the microscopic connection to the material systems (e.g., twisted MoTe₂). Developing a microscopic theory of the edge states may be useful for determining the precise conditions for the phases predicted in this work. In this work, we assume the edge state can be described by one pair of charge- e movers and one pair of charge- $e/3$. However, this is not the only edge state configuration, as the boundary may go through edge reconstruction, similar to the $\nu = 2/3$ FQH edge state [46, 72]. It is interesting to investigate the reconstructed edge theory (which contains more than two Kramers pairs) and repeat the analysis of this work. The symmetric localization is not unique to the edge states of $\nu_{\text{tot}} = 4/3$

FTI studied in this work. We note that the $\nu_{\text{tot}} = 8/3$ FTI edge state (corresponding to a $1 + 1/3$ composite helical edge [28]) also admits a similar symmetric localized state, but the required interaction corresponds to a $|\Delta S_z| = 2$ scattering. It will be useful to systematically investigate the edge-state phases and conductance values in other filling fractions, e.g., $\nu_{\text{tot}} = 4/5$. Finally, it is desirable to develop novel characterizations of the FTI beyond edge-state transport (e.g., tunneling spectroscopy and noise measurements), especially since our work provides a sharp, experimentally pertinent example that an FTI can have symmetric localized edge states.

ACKNOWLEDGMENTS

Y.-Z.C. thank Seth Musser and Yahui Zhang for useful conversations. This work is supported by the Laboratory for Physical Sciences.

Appendix A: Instability criteria and compatibility conditions

Here, we examine the TRS perturbations with Haldane’s instability criteria and the compatibility conditions [51, 55, 56]. We first provide the scattering vectors for all backscattering perturbations considered in this work and then compute the instability and compatibility conditions.

In the bosonic theory, a backscattering of fermions can be described by a vertex operator

$$\mathcal{O}_{\mathcal{X}}(\tau, x) \sim \exp[im_{\mathcal{X}}^T \Phi(\tau, x)], \quad (\text{A1})$$

where $m_{\mathcal{X}}$ is a four-component integer vector encoding the scattering. For the one-electron disorder scattering $\mathcal{S}_{I,M}$ [Eq. (4)], the scatter vectors correspond to $m_M^T = [1, 3, 0, 0]$ and $m_M^T = [0, 0, 1, 3]$. The two-electron backscattering $\mathcal{S}_{I,+}$ [Eq. (5)] corresponds to an integer-valued scattering vector $m_+^T = [1, 3, 1, 3]$. The Josephson coupling $\mathcal{S}_{I,J}$ [Eq. (6)] corresponds to an integer-valued scattering vector $m_J^T = [1, 3, -1, -3]$. The $|\Delta S_z| = 1$ two-electron interaction $\mathcal{S}_{I,\text{loc}}$ [Eq. (7)] correspond to scattering vectors $m_{\text{loc}}^T = [2, 3, 1, 0]$ and $m_{\text{loc}}^T = [1, 0, 2, 3]$.

Now, we discuss Haldane’s instability criteria and the compatibility of different perturbations [51, 55, 56]. For a scattering process described by an integer-valued scattering vector $m_{\mathcal{X}}$, the scaling dimension $\Delta(m_{\mathcal{X}})$ is bound by [43, 55, 56, 73]

$$\Delta(m_{\mathcal{X}}) \geq \left\lfloor \frac{m_{\mathcal{X}}^T \hat{\mathcal{K}}^{-1} m_{\mathcal{X}}}{2} \right\rfloor \equiv \mathcal{D}(m_{\mathcal{X}}). \quad (\text{A2})$$

When $\mathcal{D}(m_{\mathcal{X}}) = 0$, the vertex operator $e^{im_{\mathcal{X}}^T \Phi}$ can remove a pair of low-energy modes (e.g., a right-moving mode and a left-moving mode) in the strong-coupling fixed point [43, 51, 55, 56, 73]. The above situation is

Haldane's instability criteria. Using Eq. (A2), we obtain

$$\mathcal{D}(m_M) = \mathcal{D}(m'_M) = 1, \quad (\text{A3a})$$

$$\mathcal{D}(m_+) = 0, \quad (\text{A3b})$$

$$\mathcal{D}(m_J) = 0, \quad (\text{A3c})$$

$$\mathcal{D}(m_{\text{loc}}) = \mathcal{D}(m_{\text{loc}'}) = 0. \quad (\text{A3d})$$

The results above suggest that $\mathcal{S}_{I,M}$ cannot remove low energy modes in the strong-coupling limit, while other

perturbations ($\mathcal{S}_{I,+}$, $\mathcal{S}_{I,J}$, and $\mathcal{S}_{I,\text{loc}}$) satisfy the Haldane's instability criteria.

Another important question is whether two distinct perturbations are compatible. Two vertex operators, $e^{im_1^T \Phi}$ and $e^{im_2^T \Phi}$, can coexist in the strong-coupling limit if $\mathcal{C}(m_1, m_2) = m_1^T \hat{K}^{-1} m_2$. We find that $\mathcal{C}(m_M, m'_M) = \mathcal{C}(m_{\text{loc}}, m'_{\text{loc}}) = 0$ and other pairs are nonzero. Since $\mathcal{D}(m_{\text{loc}}) = \mathcal{D}(m_{\text{loc}'}) = 0$ and $\mathcal{M}(m_{\text{loc}}, m'_{\text{loc}}) = 0$, the two backscattering interactions in $\mathcal{S}_{I,\text{loc}}$ can simultaneously remove two pairs of the low-energy modes, resulting in an insulating edge state in the infinite length limit, as discussed in the main text.

* yzchou@umd.edu

- [1] B. A. Bernevig and S.-C. Zhang, Quantum Spin Hall Effect, *Phys. Rev. Lett.* **96**, 106802 (2006).
- [2] M. Levin and A. Stern, Fractional Topological Insulators, *Phys. Rev. Lett.* **103**, 196803 (2009).
- [3] J. Maciejko, X.-L. Qi, A. Karch, and S.-C. Zhang, Fractional Topological Insulators in Three Dimensions, *Phys. Rev. Lett.* **105**, 246809 (2010).
- [4] A. Stern, Fractional Topological Insulators: A Pedagogical Review, *Annual Review of Condensed Matter Physics* **7**, 349 (2016).
- [5] J. Maciejko and G. A. Fiete, Fractionalized topological insulators, *Nature Phys* **11**, 385 (2015).
- [6] T. Neupert, C. Chamon, T. Iadecola, L. H. Santos, and C. Mudry, Fractional (Chern and topological) insulators, *Phys. Scr.* **2015**, 014005 (2015).
- [7] M. Cheng, Superconducting proximity effect on the edge of fractional topological insulators, *Phys. Rev. B* **86**, 195126 (2012).
- [8] J. Klinovaja, A. Yacoby, and D. Loss, Kramers pairs of Majorana fermions and parafermions in fractional topological insulators, *Phys. Rev. B* **90**, 155447 (2014).
- [9] J. Alicea and P. Fendley, Topological Phases with Parafermions: Theory and Blueprints, *Annual Review of Condensed Matter Physics* **7**, 119 (2016).
- [10] F. Wu, T. Lovorn, E. Tutuc, and A. H. MacDonald, Hubbard Model Physics in Transition Metal Dichalcogenide Moiré Bands, *Phys. Rev. Lett.* **121**, 026402 (2018).
- [11] F. Wu, T. Lovorn, E. Tutuc, I. Martin, and A. H. MacDonald, Topological Insulators in Twisted Transition Metal Dichalcogenide Homobilayers, *Phys. Rev. Lett.* **122**, 086402 (2019).
- [12] H. Pan, F. Wu, and S. Das Sarma, Quantum phase diagram of a Moiré model, *Phys. Rev. B* **102**, 201104 (2020).
- [13] H. Pan, M. Xie, F. Wu, and S. Das Sarma, Topological Phases in AB-Stacked MoTe₂/WSe₂: \mathbb{Z}_2 Topological Insulators, Chern Insulators, and Topological Charge Density Waves, *Phys. Rev. Lett.* **129**, 056804 (2022).
- [14] M. Xie, H. Pan, F. Wu, and S. Das Sarma, Nematic Excitonic Insulator in Transition Metal Dichalcogenide Moiré Heterobilayers, *Phys. Rev. Lett.* **131**, 046402 (2023).
- [15] K. F. Mak and J. Shan, Semiconductor moiré materials, *Nat. Nanotechnol.* **17**, 686 (2022).
- [16] B. Li, W.-X. Qiu, F. Wu, and A. H. MacDonald, Quantum phases in twisted homobilayer transition metal dichalcogenides, *Nat Sci Rev* **13**, nwaf570 (2026).
- [17] J. Cai, E. Anderson, C. Wang, X. Zhang, X. Liu, W. Holtzmann, Y. Zhang, F. Fan, T. Taniguchi, K. Watanabe, Y. Ran, T. Cao, L. Fu, D. Xiao, W. Yao, and X. Xu, Signatures of fractional quantum anomalous Hall states in twisted MoTe₂, *Nature* **622**, 63 (2023).
- [18] Y. Zeng, Z. Xia, K. Kang, J. Zhu, P. Knüppel, C. Vaswani, K. Watanabe, T. Taniguchi, K. F. Mak, and J. Shan, Thermodynamic evidence of fractional Chern insulator in moiré MoTe₂, *Nature* **622**, 69 (2023).
- [19] H. Park, J. Cai, E. Anderson, Y. Zhang, J. Zhu, X. Liu, C. Wang, W. Holtzmann, C. Hu, Z. Liu, T. Taniguchi, K. Watanabe, J.-H. Chu, T. Cao, L. Fu, W. Yao, C.-Z. Chang, D. Cobden, D. Xiao, and X. Xu, Observation of fractionally quantized anomalous Hall effect, *Nature* **622**, 74 (2023).
- [20] F. Xu, Z. Sun, T. Jia, C. Liu, C. Xu, C. Li, Y. Gu, K. Watanabe, T. Taniguchi, B. Tong, J. Jia, Z. Shi, S. Jiang, Y. Zhang, X. Liu, and T. Li, Observation of Integer and Fractional Quantum Anomalous Hall Effects in Twisted Bilayer $\{\text{MoTe}\}_2$, *Phys. Rev. X* **13**, 031037 (2023).
- [21] F. Xu, Z. Sun, J. Li, C. Zheng, C. Xu, J. Gao, T. Jia, K. Watanabe, T. Taniguchi, B. Tong, L. Lu, J. Jia, Z. Shi, S. Jiang, Y. Zhang, Y. Zhang, S. Lei, X. Liu, and T. Li, Signatures of unconventional superconductivity near reentrant and fractional quantum anomalous Hall insulators (2025), [arXiv:2504.06972 \[cond-mat\]](https://arxiv.org/abs/2504.06972).
- [22] K. Kang, B. Shen, Y. Qiu, Y. Zeng, Z. Xia, K. Watanabe, T. Taniguchi, J. Shan, and K. F. Mak, Evidence of the fractional quantum spin Hall effect in moiré MoTe₂, *Nature*, 1 (2024).
- [23] Y.-H. Zhang, Vortex Spin Liquid with Fractional Quantum Spin Hall Effect in Moiré Chern Bands, *Phys. Rev. Lett.* **133**, 106502 (2024).
- [24] C.-M. Jian, M. Cheng, and C. Xu, Minimal Fractional Topological Insulator in Half-Filled Conjugate Moiré Chern Bands, *Phys. Rev. X* **15**, 021063 (2025).
- [25] Y.-H. Zhang, Non-Abelian and Abelian descendants of a vortex spin liquid: Fractional quantum spin Hall effect in twisted MoTe₂, *Phys. Rev. B* **110**, 155102 (2024).
- [26] J. May-Mann, A. Stern, and T. Devakul, Theory of half-integer fractional quantum spin Hall edges, *Phys. Rev. B* **111**, L201111 (2025).
- [27] I. Sodemann Villadiego, Halperin states of particles and holes in ideal time reversal invariant pairs of Chern bands and the fractional quantum spin Hall effect in moiré

- MoTe₂, *Phys. Rev. B* **110**, 045114 (2024).
- [28] Y.-Z. Chou and S. Das Sarma, Composite helical edges from Abelian fractional topological insulators, *Phys. Rev. B* **110**, 155117 (2024).
- [29] A. P. Reddy, N. Paul, A. Abouelkomsan, and L. Fu, Non-Abelian Fractionalization in Topological Minibands, *Phys. Rev. Lett.* **133**, 166503 (2024).
- [30] R. Wen and A. C. Potter, *Cheshire qudits from fractional quantum spin Hall states in twisted MoTe₂* (2024), arXiv:2407.03401 [cond-mat].
- [31] Y. H. Kwan, G. Wagner, J. Yu, A. K. Dagnino, Y. Jiang, X. Xu, B. A. Bernevig, T. Neupert, and N. Regnault, Regarding the existence of abelian fractional topological insulators in twisted MoTe₂ and related systems, *Commun Phys* **9**, 52 (2026).
- [32] F. Chen, W.-W. Luo, W. Zhu, and D. N. Sheng, *Robust non-Abelian even-denominator fractional Chern insulator in twisted bilayer MoTe₂* (2024), arXiv:2405.08386 [cond-mat].
- [33] C. Xu, N. Mao, T. Zeng, and Y. Zhang, Multiple Chern Bands in Twisted MoTe₂ and Possible Non-Abelian States, *Phys. Rev. Lett.* **134**, 066601 (2025).
- [34] T. Lu, Y.-M. Wu, and L. H. Santos, Electromagnetic response and emergent topological orders in transition metal dichalcogenide MoTe₂ bilayers, *Phys. Rev. B* **112**, 085138 (2025).
- [35] H. Park, J. Cai, E. Anderson, X.-W. Zhang, X. Liu, W. Holtzmann, W. Li, C. Wang, C. Hu, Y. Zhao, T. Taniguchi, K. Watanabe, J. Yang, D. Cobden, J.-H. Chu, N. Regnault, B. A. Bernevig, L. Fu, T. Cao, D. Xiao, and X. Xu, *Ferromagnetism and Topology of the Higher Flat Band in a Fractional Chern Insulator* (2024), arXiv:2406.09591 [cond-mat].
- [36] F. Xu, X. Chang, J. Xiao, Y. Zhang, F. Liu, Z. Sun, N. Mao, N. Peshcherenko, J. Li, K. Watanabe, T. Taniguchi, B. Tong, L. Lu, J. Jia, D. Qian, Z. Shi, Y. Zhang, X. Liu, S. Jiang, and T. Li, Interplay between topology and correlations in the second moiré band of twisted bilayer MoTe₂, *Nat. Phys.* **21**, 542 (2025).
- [37] L. An, H. Pan, W.-X. Qiu, N. Wang, S. Ru, Q. Tan, X. Dai, X. Cai, Q. Shang, X. Lu, H. Jiang, X. Lyu, S. Yang, K. Watanabe, T. Taniguchi, F. Wu, and W.-b. Gao, Observation of ferromagnetic phase in the second moiré band of twisted MoTe₂, *Nat Commun* **16**, 5131 (2025).
- [38] K. Kang, Y. Qiu, B. Shen, K. Lee, Z. Xia, Y. Zeng, K. Watanabe, T. Taniguchi, J. Shan, and K. F. Mak, *Time-reversal symmetry breaking fractional quantum spin Hall insulator in moiré MoTe₂* (2025), arXiv:2501.02525 [cond-mat].
- [39] Y. Wang, G. E. Minarik, W. Li, Y. Kwan, S. Yuan, E. Anderson, C. Hu, J. Ingham, J. Choe, T. Taniguchi, K. Watanabe, X. Roy, J.-H. Chu, R. Queiroz, J. C. Hone, N. Regnault, X. Xu, and X. Zhu, *Magnetic Signatures of a Putative Fractional Topological Insulator in Twisted MoTe₂* (2026), arXiv:2601.18508 [cond-mat].
- [40] S. Musser, M. Cheng, and T. Senthil, Fractionalization as an alternate to charge ordering in electronic insulators, *Phys. Rev. B* **111**, 235108 (2025).
- [41] X. G. Wen and A. Zee, Classification of Abelian quantum Hall states and matrix formulation of topological fluids, *Phys. Rev. B* **46**, 2290 (1992).
- [42] A. M. Chang, Chiral Luttinger liquids at the fractional quantum Hall edge, *Rev. Mod. Phys.* **75**, 1449 (2003).
- [43] T. Neupert, L. Santos, S. Ryu, C. Chamon, and C. Mudry, Fractional topological liquids with time-reversal symmetry and their lattice realization, *Phys. Rev. B* **84**, 165107 (2011).
- [44] C. L. Kane, M. P. A. Fisher, and J. Polchinski, Randomness at the edge: Theory of quantum Hall transport at filling $\nu = 2/3$, *Phys. Rev. Lett.* **72**, 4129 (1994).
- [45] I. V. Protopopov, Y. Gefen, and A. D. Mirlin, Transport in a disordered $\nu = 2/3$ fractional quantum Hall junction, *Annals of Physics* **385**, 287 (2017).
- [46] C. Nosiglia, J. Park, B. Rosenow, and Y. Gefen, Incoherent transport on the $\nu = 2/3$ quantum Hall edge, *Phys. Rev. B* **98**, 115408 (2018).
- [47] T. Giamarchi and H. J. Schulz, Anderson localization and interactions in one-dimensional metals, *Phys. Rev. B* **37**, 325 (1988).
- [48] T. Giamarchi, *Quantum Physics in One Dimension* (Clarendon Press, 2003).
- [49] C. L. Kane and M. P. A. Fisher, Impurity scattering and transport of fractional quantum Hall edge states, *Phys. Rev. B* **51**, 13449 (1995).
- [50] C. L. Kane and M. P. A. Fisher, Contacts and edge-state equilibration in the fractional quantum Hall effect, *Phys. Rev. B* **52**, 17393 (1995).
- [51] F. D. M. Haldane, Stability of Chiral Luttinger Liquids and Abelian Quantum Hall States, *Phys. Rev. Lett.* **74**, 2090 (1995).
- [52] A. O. Gogolin, A. A. Nersesyan, and A. M. Tsvelik, *Bosonization and Strongly Correlated Systems* (Cambridge University Press, 2004).
- [53] Y. Oreg, E. Sela, and A. Stern, Fractional helical liquids in quantum wires, *Phys. Rev. B* **89**, 115402 (2014).
- [54] J. I. Väyrynen, M. Goldstein, and Y. Gefen, Superconductivity of neutral modes in quantum Hall edges, *Phys. Rev. B* **105**, L081402 (2022).
- [55] J. E. Moore and X.-G. Wen, Critical points in edge tunneling between generic fractional quantum Hall states, *Phys. Rev. B* **66**, 115305 (2002).
- [56] C. Xu and J. E. Moore, Stability of the quantum spin Hall effect: Effects of interactions, disorder, and \mathbb{Z}_2 topology, *Phys. Rev. B* **73**, 045322 (2006).
- [57] H.-Y. Xie, H. Li, Y.-Z. Chou, and M. S. Foster, Topological Protection from Random Rashba Spin-Orbit Backscattering: Ballistic Transport in a Helical Luttinger Liquid, *Phys. Rev. Lett.* **116**, 086603 (2016).
- [58] C. Wu, B. A. Bernevig, and S.-C. Zhang, Helical Liquid and the Edge of Quantum Spin Hall Systems, *Phys. Rev. Lett.* **96**, 106401 (2006).
- [59] C. L. Kane and E. J. Mele, Quantum Spin Hall Effect in Graphene, *Phys. Rev. Lett.* **95**, 226801 (2005).
- [60] M. Z. Hasan and C. L. Kane, Colloquium: Topological insulators, *Rev. Mod. Phys.* **82**, 3045 (2010).
- [61] X.-L. Qi and S.-C. Zhang, Topological insulators and superconductors, *Rev. Mod. Phys.* **83**, 1057 (2011).
- [62] C. L. Kane, R. Mukhopadhyay, and T. C. Lubensky, Fractional Quantum Hall Effect in an Array of Quantum Wires, *Phys. Rev. Lett.* **88**, 036401 (2002).
- [63] J. C. Y. Teo and C. L. Kane, From Luttinger liquid to non-Abelian quantum Hall states, *Phys. Rev. B* **89**, 085101 (2014).
- [64] Y.-Z. Chou and S. Das Sarma, Correlated insulator in two Coulomb-coupled quantum wires, *Phys. Rev. B* **108**, 235135 (2023).
- [65] M. Levin and A. Stern, Classification and analysis of

- two-dimensional Abelian fractional topological insulators, *Phys. Rev. B* **86**, 115131 (2012).
- [66] T. L. Schmidt, S. Rachel, F. von Oppen, and L. I. Glazman, Inelastic Electron Backscattering in a Generic Helical Edge Channel, *Phys. Rev. Lett.* **108**, 156402 (2012).
- [67] N. Lezmy, Y. Oreg, and M. Berkooz, Single and multiparticle scattering in helical liquid with an impurity, *Phys. Rev. B* **85**, 235304 (2012).
- [68] Y.-Z. Chou, A. Levchenko, and M. S. Foster, Helical Quantum Edge Gears in 2D Topological Insulators, *Phys. Rev. Lett.* **115**, 186404 (2015).
- [69] N. Kainaris, I. V. Gornyi, S. T. Carr, and A. D. Mirlin, Conductivity of a generic helical liquid, *Phys. Rev. B* **90**, 075118 (2014).
- [70] N. Kainaris, I. V. Gornyi, A. Levchenko, and D. G. Polyakov, Coulomb drag between helical Luttinger liquids, *Phys. Rev. B* **95**, 045150 (2017).
- [71] X. Zhang and M. S. Foster, Dissipative Hot-Spot-Enabled Shock and Bounce Dynamics via Terahertz Quantum Quenches in Helical Edge States, *Phys. Rev. Lett.* **127**, 026801 (2021).
- [72] J. Wang, Y. Meir, and Y. Gefen, Edge Reconstruction in the $\nu = 2/3$ Fractional Quantum Hall State, *Phys. Rev. Lett.* **111**, 246803 (2013).
- [73] T. Neupert, C. Chamon, C. Mudry, and R. Thomale, Wire deconstructionism of two-dimensional topological phases, *Phys. Rev. B* **90**, 205101 (2014).